frontiers | Frontiers in Built Environment

TYPE Original Research
PUBLISHED 13 November 2025
DOI 10.3389/fbuil.2025.1695449

OPEN ACCESS

EDITED BY
Adel Juaidi,
An-Najah National University, Palestine

REVIEWED BY
Ramez Abdallah,
An-Najah National University, Palestine
En Li,
Henan University of Technology, China

*CORRESPONDENCE
Szende Szentesi-Nejur,
szende.szentesi-nejur@arc.ulaval.ca

RECEIVED 29 August 2025
REVISED 17 October 2025
ACCEPTED 24 October 2025
PUBLISHED 13 November 2025

CITATION
Harvey G and Szentesi-Nejur S (2025) Field-based thermal performance analysis of a cement-stabilized, core-insulated rammed earth house in a cold climate.
Front. Built Environ. 11:1695449.
doi: 10.3389/fbuil.2025.1695449

Field-based thermal performance analysis of a cement-stabilized, core-insulated rammed earth house in a cold climate

Gabriel Harvey and Szende Szentesi-Nejur*

Université Laval, Faculté d'aménagement, d'architecture, d'art et de design, Québec City, QC, Canada

This study presents an exploratory, in-depth case study on the short-term thermal and hygrothermal performance of a cement-stabilized, core-insulated rammed earth house in a cold-climate region of eastern Canada. Rammed earth construction is increasingly promoted as an eco-efficient solution for winter-dominated climates due to its thermal and moisture-regulating properties, however, empirical validation under real-world conditions remains limited. A three-day monitoring campaign was conducted under free-running winter conditions using three complementary methods: infrared thermography (IRT), surface heat flux sensing, and *in-situ* temperature and humidity measurements. The results reveal measurable thermal lag, reduced diurnal temperature swings, and delayed heat dissipation during unheated periods, indicating high passive heat retention. IRT demonstrated dynamic surface temperature responses to solar exposure, particularly on the south-facing wall, while heat flux data confirmed reduced transmittance through the composite earthen envelope. Indoor temperature and relative humidity remained stable throughout the monitoring period, reflecting effective hygrothermal buffering. Although limited in duration and scope, this study provides a rare, high-resolution benchmark dataset that characterizes the short-term behavior of insulated rammed earth walls in cold climates and supports future simulation-based and long-term field investigations.

KEYWORDS

rammed earth construction, cold-climate performance, thermal mass effect, hygrothermal buffering, building envelope analysis, on-site monitoring, infrared thermography (IRT), surface heat flux measurement

1 Introduction

Rammed earth construction is increasingly considered a viable solution in cold climate for energy-efficient and low-impact buildings, offering significant thermal inertia, hygrothermal regulation, and low embodied energy (Easton, 2007; Hall and Allinson, 2012; Krahn, 2019). Numerous studies have highlighted the ability of rammed earth's thermal mass to enhance energy efficiency by storing heat and releasing it gradually

(Beckett and Ciancio, 2012; Dong et al., 2014; Fernandes et al., 2019; Samadianfard and Toufigh, 2020; Soudani et al., 2017; Uprety et al., 2024). However, most performance evaluations have been carried out in warm or temperate climates, where its passive thermal behavior has been shown to reduce reliance on active systems (Dong et al., 2014; Beckett et al., 2017; Gupta et al., 2020). Recent reports in Canada highlight the energy-related benefits of rammed earth (Ciancio and Beckett, 2015; Krayenhoff, 2012; Wong and Cook, 2014), but they often lack a clear methodological framework or detailed explanation of data sources, which limits the reliability of their findings. Nonetheless, the observations presented in these reports, based on 30-day monitoring periods, demonstrate the material's ability to slow heat loss and moderate indoor temperatures in unoccupied dwellings, underscoring its capacity to dampen thermal fluctuations and capitalize on thermal mass effects (Krayenhoff, 2012; Wong and Cook, 2014).

Although several simulation-based studies have explored the thermal performance of rammed earth in cold-climate settings (Fix and Richman, 2009; Yu et al., 2022), there is a lack of rigorous field-based investigations that assess the combined hygrothermal and thermal behavior under real-world conditions. Moreover, comparisons between simulated and real-world projects have revealed that simulations often overestimate performance, with results not fully reflected in practice (Beckett et al., 2017; Mellado et al., 2021; Taylor et al., 2008). One example would be the durability-related issues, such as moisture accumulation and freeze–thaw degradation, which remain insufficiently studied in cold-climate contexts (Rempel and Rempel, 2019). Field-based evidence has documented cases of wall deterioration occurring within only a few years of construction (Kailey and Rishi, 2015), potentially compromising the key hygrothermal and structural properties of the rammed earth envelope.

Rammed earth walls are valued for their thermal inertia but possess low thermal resistance due to their moderate to high thermal conductivity (Hall and Allinson, 2009). Field-based studies have revealed that uninsulated rammed earth walls are prone to significant heat loss, limiting their applicability in cold climate regions (Dong et al., 2014; Mellado et al., 2021). To address this, the addition of insulation is widely recognized as the most effective strategy for enhancing thermal performance and delaying heat transfer. This has been demonstrated by laboratory experiments (Hall and Allinson, 2009; Jiang et al., 2020), building-scale simulations (Dong et al., 2014; Gupta et al., 2020; Hasan and Dutta, 2015), and field research validated through cross-verification methods (Beckett et al., 2017; Mellado et al., 2021; Serrano et al., 2016). It is important to note that in cold climates, one of the key aspects of energy-efficient envelope design is insulation, along with airtightness, as both are essential to reducing conductive heat loss and maintaining indoor thermal comfort (Hutcheon and GOP, 1995).

In North America, core insulation is commonly employed to preserve the aesthetic of exposed rammed earth on both interior and exterior wall surfaces (Krahn, 2019), despite evidence indicating that external insulation is more thermally efficient (Fix and Richman, 2009; Yu et al., 2022). Studies have shown that external insulation can improve indoor thermal performance is also suggested to reduce environmental moisture absorption and protect against freeze–thaw damage (Gupta et al., 2020; Fix and Richman, 2009; Yu et al., 2022). Nevertheless, core insulation has been reported to offer longer periods of thermal comfort and smaller indoor temperature fluctuations compared to other insulation strategies (Tinsley et al., 2019).

To address moisture accumulation and freeze–thaw deterioration, cold-climate adaptations often include cement stabilization, binding agents, and water-repellent additives. While these additions enhance structural durability and moisture resistance, the use of cementitious binders has been shown to reduce the material's hygroscopic capacity, diminishing its ability to buffer indoor humidity (Hall and Allinson, 2012; Arrigoni et al., 2017; Narloch et al., 2019). Although this reduction in vapor uptake may slightly improve thermal resistance by decreasing conductive heat transfer, it also compromises one of the key passive regulation benefits of traditional rammed earth construction.

Even with appropriate wall composition to ensure thermal performance in cold climates (Dong et al., 2014), both field and simulation based studies demonstrate that energy-efficient buildings depend on bioclimatic design tailored to local climate, site, and function (Taylor et al., 2008; Giuffrida et al., 2021). Orientation and window-to-wall ratios (WWR) are especially critical, as passive solar gains and reduced heat transmittance can significantly improve energy efficiency (Hasan and Dutta, 2015; Dong et al., 2015). In cold regions, envelope detailing to achieving airtightness is also a key factor in improving energy performance (Hutcheon and GOP, 1995), which is also emphasised for rammed earth construction (Krayenhoff, 2012).

To assess the thermal behavior of rammed earth envelopes, key parameters such as temperature and humidity have been commonly monitored in the research field to evaluate indoor climate stability, thermal inertia, and heat retention capacity (Fernandes et al., 2019; Mellado et al., 2021; Taylor et al., 2008; Taylor and Luther, 2004). Surface temperature and heat flux monitoring have proven valuable for providing real-time, quantitative data on heat transfer, allowing assessment of insulation performance, thermal mass efficiency, and energy retention (Samadianfard and Toufigh, 2020; Taylor et al., 2008; Verbeke and Audenaert, 2018). These techniques also support analysis of heat storage and release dynamics (Samadianfard and Toufigh, 2020; Soudani et al., 2017).

The identification of thermal anomalies, such as surface temperature irregularities, thermal bridges, and insulation defects, further aids in diagnosing heat loss through the building envelope (Martin et al., 2022). IRT has become a widely accepted non-invasive method for detecting these anomalies (Martin et al., 2022). IRT has also proven effective for mapping surface temperature distributions and assessing time- and orientation-dependent behavior of wall assemblies, offering valuable insights into their overall thermal performance under fluctuating environmental conditions (Uprety et al., 2024). Although widely used in energy audits, the broader application of this approach to rammed earth buildings remains limited, most studies have focused either on energy performance in hot-climate contexts (Uprety et al., 2024) or on heritage preservation (Balaguer et al., 2019).

Although rammed earth construction is increasingly promoted as a sustainable and energy-efficient envelope solution, its actual thermal and hygrothermal performance under cold-climate

conditions remains insufficiently validated through field-based studies. Most existing research relies on numerical simulations or laboratory-scale testing, often failing to capture the combined effects of real environmental variability, material behavior, and construction detailing. Empirical data from full-scale monitoring campaigns are particularly scarce in North America, where cold and highly variable climates pose unique challenges for earth-based construction.

This article addresses this gap by presenting one of the few *in-situ*, multi-method monitoring studies of a contemporary cement-stabilized, core-insulated rammed earth building in a cold climate. Through the integration of infrared thermography, heat flux sensing, and *in-situ* hygrothermal monitoring under free-running winter conditions, the research provides high-resolution empirical evidence of short-term thermal lag, directional heat flow, and humidity stability in real operation. The study's originality lies in documenting the dynamic thermal response of insulated rammed earth walls under field conditions, offering a rare benchmark dataset that can support the calibration of future simulations and the design of energy-efficient, climate-responsive earthen envelopes.

2 Materials and methods

The research methodology (Figure 1) integrates experimental setup, controlled preconditioning, multi-sensor field monitoring, and data synthesis within a structured sequence. The field campaign was conducted on a full-scale cement-stabilized, core-insulated rammed earth residence in southern Ontario to evaluate its short-term thermal and hygrothermal response under representative winter conditions. Following sensor calibration and thermal stabilization, the building was transitioned to a free-running state to isolate envelope-driven dynamics. Infrared thermography, surface heat-flux sensing, and *in-situ* temperature and humidity monitoring were deployed concurrently to capture thermal lag, diurnal stability, and hygrothermal buffering. Data acquisition combined automated and manual systems, followed by synchronization, averaging, and cross-validation of datasets. This integrative framework ensured a comprehensive and reproducible assessment of the envelope's passive performance, linking *in-situ* evidence to material and environmental parameters.

2.1 Case study description

The selected case study is a single-story guest house, physically connected to the main residence by a continuous roof forming a covered entry and parking area. Located in southern Ontario, the building is constructed with cement-stabilized rammed earth walls incorporating a core insulation layer. The load-bearing walls are reinforced with steel rebar placed on both the interior and exterior faces to enhance structural integrity while preserving the monolithic appearance of the wall assembly (Figure 2). A continuous core insulation layer, composed of 152 mm thick foam board, is integrated within the wall profile to improve thermal resistance and minimize heat loss without compromising the wall's thermal inertia. The full assembly results in a consistent wall thickness of 508 mm, which facilitates comparative analysis of thermal behavior across different orientations. Table 1 summarizes the wall assemblies and material properties, while Table 2 outlines the boundary conditions applied during the monitoring period. The building layout is compact and symmetrical, allowing for orientation-based monitoring of thermal performance. The house features two main bedrooms located on the north and south sides of the plan respectively (Figure 3). These spaces are separated by a central main area, which include the kitchen and open on the bathroom and mechanical room to the north. All interior spaces are exposed to varying degrees of solar radiation depending on their position. The primary façade faces south, with a window-to-wall ratio (WWR) of approximately 19%. The east façade has a WWR of about 7%, the north façade less than 10%, and the west façade has no fenestration. This distribution maximizes passive solar gains on the south side while limiting winter heat losses on other orientations. The building's footprint and envelope allow for controlled monitoring of thermal gradients across interior and exterior zones and all wall orientations.

2.2 Infrared thermography protocol

IRT was used throughout the experiment to monitor surface temperature variations and assess insulation performance across all wall orientations, both interior and exterior (Figure 4), capturing spatial temperature differences and identifying thermal bridges at critical junctions such as wall intersections, window perimeters, and foundation-wall interfaces. Scans were conducted at eight fixed time intervals per day, 03:00, 06:00, 09:00, 12:00, 15:00, 18:00, 21:00, and 00:00, to document the full diurnal cycle, including deep nocturnal cooling, peak solar exposure, and residual nighttime heat dissipation.

Thermographic data were collected using a HIKMICRO B10S thermal camera (640 × 480 resolution, ±2% accuracy), with a standardized emissivity value of 0.95 and concurrent logging of ambient environmental conditions. To ensure consistent image acquisition, reflective markers were placed on the wall surface and floor markers were used to position the tripod across all sessions. Temperatures at the center of each image, aligned with reflective markers and adjacent to heat flux sensors, were recorded to allow direct comparison with thermal flux data (Figure 5). This protocol enabled high-precision spatial and temporal analysis of the wall's thermal behavior.

2.3 Heat flux monitoring

As recommended in ISO 6781-1, 2023, IRT was complemented by another monitoring method, in this case, heat flux measurements, to enable direct comparison of data across all monitored wall sections. Heat flux sensors were installed on representative wall sections for all orientations, with paired sensors mounted directly opposite each other on the interior and exterior surfaces to capture directional heat flow across the building envelope. Each sensor was positioned on an even surface and shielded to minimize the effects of direct solar radiation and air currents (Figure 6). Two sensor types were employed: four FluxTeq PHFS-01 units with

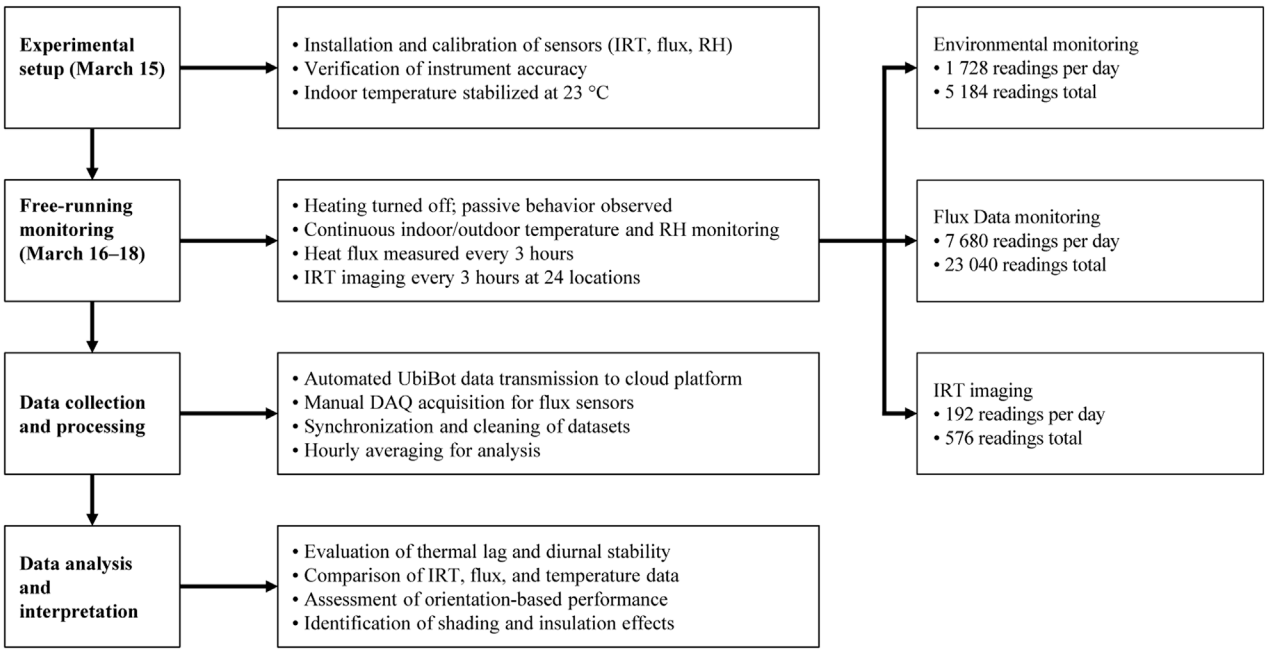

FIGURE 1
Methodological workflow.

FIGURE 2
Front view and wall section of the case study house upon arrival on March 15, showing the exposed rammed earth façade and the internal composition of the 508 mm thick sandwich wall system with cement-stabilized earth and core insulation.

a 1″× 1″sensing area and four PHFS-OEM units with a 0.5″× 0.5″area, both of which are thin and flexible to allow for discreet surface mounting.

All sensors were connected to a FluxTeq Compaq data acquisition system (DAQ), which was interfaced with a laptop for data logging and control. This setup enabled detailed monitoring of the thermal mass effect, specifically, how heat was absorbed, stored, and released during heating and cooling cycles, and supported comparisons between solar-exposed and shaded walls to highlight variations in solar gain and heat loss. Measurements were taken every 3 h, with each session lasting 1 min; data were averaged to reduce short-term fluctuations due to air movement or electronic noise. This ensured consistent and time-aligned thermal profiles across all surfaces, allowing robust evaluation of insulation performance, thermal inertia, and diurnal heat exchange behavior.

TABLE 1 Building envelope assemblies and thermal properties.

Elements	Assembly description (Interior – Exterior)	Thickness (mm)	U-value (W/(m^2·K)) *Estimated at construction
Foundation	Concrete foundations with 6″ of rigid insulation	480 mm	0.045
Exterior walls	6″ Rigid insulation between two rammed earth walls (6″ exterior veneer wall and 8″ interior structural wall)	508 mm	0.033
Roof	16″ dense packed cellulose between roof joists, with vapour permeable air barrier	450 mm	0.017
Slab	Marmoleum flooring on plywood slab, with underslab vapour barrier and 10″ rigid insulation	250 mm	0.027
Windows	Triple-pane with Argon gas infill w/SHGC of 0.63. Include External Solar Shading on South-facing windows	Triple-pane	0.147
Doors	Model unknown. Window: Triple-pane with Argon gas infill w/SHGC of 0.63	Triple-latch Seal	0.083

TABLE 2 Boundary conditions during the monitoring period.

Boundary condition	Description
Occupancy/internal gains	• House was occupied by the researcher during the monitoring period • Appliances and equipment used or in operation: refrigerator, micro-wave, lights, monitoring devices, laptops, cellphone chargers
Heating schedule	• Interior heated to 23 °C until March 15, after which the building was left in free-running mode (March 16–18)
Ventilation/infiltration	• No ventilation system was active during the monitoring period • The exterior door was briefly opened twice every 3 h to allow for equipment relocation between interior and exterior measurements. However, as the door opened onto an insulated vestibule, direct thermal exchange with the outdoor environment was minimized • The heat flux sensor wires were routed through 2 windows (south and north) to connect to the data acquisition computer. The windows were firmly closed around the cables to minimize air infiltration during the monitoring period • Airtightness testing was not performed as part of this study
House design	• Permanent overhang present on west façade reduce afternoon solar exposure. This influenced west wall performance and is briefly discussed in Section 4.4 • An insulated porch is attached to the west facing wall of the house, which can limit the analysis on this wall

2.4 Environmental monitoring

To assess thermal response and hygrothermal behavior, indoor and outdoor temperature and RH were recorded every 10 min during the three-day measurement using UbiBot RS485 TH30S-B probes and UbiBot wireless sensor WS1 Pro data loggers. All sensors were mounted on tripods positioned at the center of their respective rooms to minimize the influence of localized thermal anomalies, such as proximity to walls, windows, or heat sources, and to provide a more accurate representation of overall room conditions (Figure 7).

Although raw data were collected at 10-min intervals, hourly averages were calculated to filter out transient fluctuations and capture longer-term thermal and moisture trends relevant to passive performance evaluation. Indoor temperature readings were used to assess the influence of thermal inertia and passive heat retention during unheated periods, while outdoor measurements provided the baseline for identifying thermal gradients across the envelope. Concurrent RH tracking offered insight into indoor moisture stability and potential condensation risks, especially under conditions of high exterior variability. Although no sensors were embedded within the wall structure, the contrast between indoor and outdoor data yielded meaningful information on the envelope's buffering capacity.

2.5 Climatic context

To contextualize environmental variations during the experimental window, additional climatic data were retrieved from the nearest weather station of The Meteorological Service of Canada (MSC). This dataset confirmed substantial snowmelt and a shift

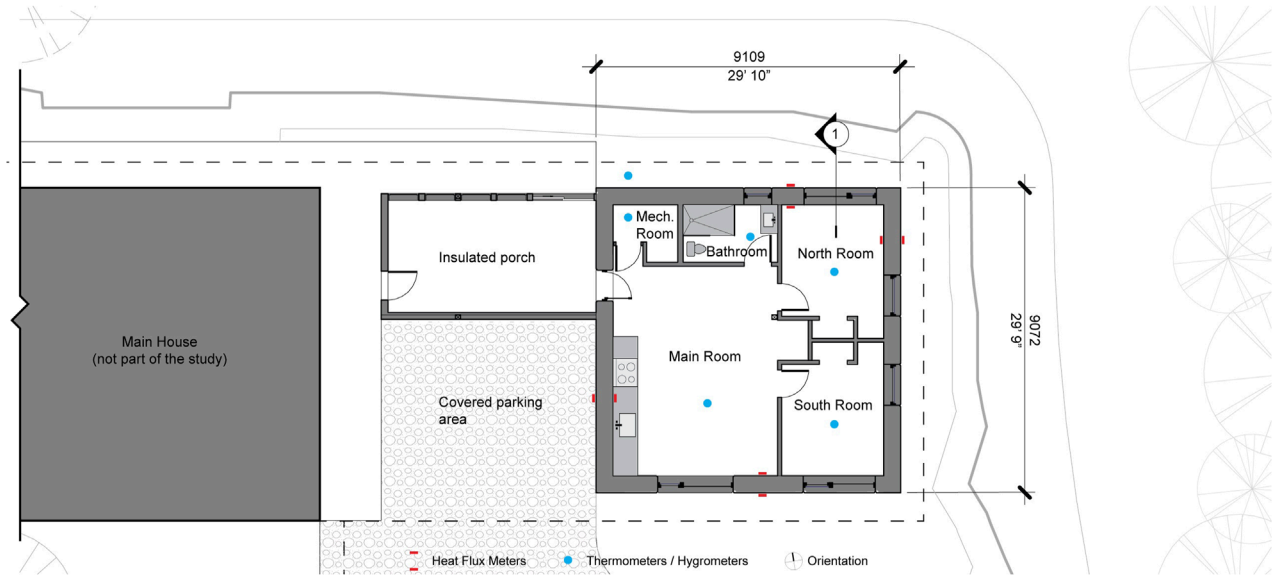

FIGURE 3
Plan view of the case study house showing room layout and orientation. The symmetrical configuration facilitates orientation-based monitoring of thermal behavior across different interior zones.

from mixed precipitation and storms to clear, sunny weather with stable outdoor temperatures. These variable conditions enabled the examination of wall performance under contrasting solar gain, ambient temperature, and humidity profiles. A photographic record of the front yard illustrates progressive snow disappearance between March 15 and 20 (Figure 8), while the climate station data further characterizes wind speed, precipitation, and cloud cover (Figure 9). Together, these environmental inputs framed the interpretation of heat flux and thermal imaging results, contributing to a comprehensive understanding of passive and active thermal dynamics in the case study home.

3 Results

This section presents an analysis of the thermal performance of the cement-stabilized, core-insulated rammed earth wall under passive conditions during the unheated period (March 16–18, 2025). Results are structured in accordance with the monitoring methods and temporal progression of solar and ambient conditions.

3.1 Wall surface temperature trends

Surface temperature data collected via IRT across all exterior wall orientations reveal clear patterns of diurnal variation influenced by solar exposure, wall orientation, and ambient conditions (Figure 10). The monitoring period (March 16–18, 2025) included both overcast and sunny conditions, offering a comparative basis for evaluating solar gain, heat retention, and thermal lag.

On March 16, a partially sunny day, all façades experienced gradual warming between 06:00 and 15:00, with surface temperatures peaking in the afternoon before cooling toward evening. The south-facing wall exhibited the strongest solar responsiveness: segment points *South Wall 2 Ext.* and *South Wall 1 Ext.* reached 9.6 °C and 8.9 °C respectively at 15:00, both slightly below the corresponding outdoor air temperature of approximately 12 °C. This indicates a measurable capacity of the rammed earth envelope to absorb shortwave radiation under moderate solar input.

March 17, in contrast, was fully overcast, resulting in a consistent surface cooling trend throughout the day and into the night. Wall temperatures dropped steadily, with early-morning lows between −4 °C and −8 °C recorded at 06:00 on March 18. As expected, south-facing walls cooled more slowly, while east- and north-facing walls showed sharper declines due to lower exposure.

March 18, the sunniest day, produced the most pronounced diurnal response. *South Wall 3 Ext.* peaked at 23.9 °C by 15:00, approximately 6 °C–8 °C above ambient. East and West-facing walls followed with smaller gains: *East Wall 3 Ext.* reached 9.3 °C, while *West Wall 2 Ext.* peaked at 9.5 °C. Within the West-facing wall, two measurement points showed distinct behavior, *West Wall 2 Ext.* displayed patterns similar to the east wall due to partial solar exposure, reaching higher surface temperatures, whereas *West Wall 1 Ext.*, fully shaded by the roof overhang and attached porch, remained significantly cooler. The north wall showed minimal variation, peaking at ~6.7 °C. These results point to substantial direct solar gain on exposed walls and the envelope's ability to store and gradually re-emit heat throughout the evening.

This behavior is illustrated by the south wall IRT sequence on March 18 (Figure 11). The images reveal color transitions corresponding to early morning warming, peak midday solar gain, and slower evening cooling. Despite outdoor air temperatures

FIGURE 4
Visual images showing the 24 interior and exterior wall segments scanned at fixed time intervals throughout the diurnal monitoring cycle. Segment name tags correspond to those referenced in Section 3.1 for the analysis of surface temperature trends.

FIGURE 5
Monitoring setup for infrared thermography, illustrating the use of wall and floor markers to standardize image acquisition across all measurement intervals.

FIGURE 6
Heat flux sensor mounted on the exterior surface of the west-facing wall, with wiring routed through the window frame to connect with the FluxTeq Compaq DAQ system located indoors.

dropping below 5 °C by 21:00, surface temperatures on the south wall remained visibly elevated, indicating significant short-term heat retention in the exterior mass.

Interior surfaces, by comparison, remained remarkably stable. As shown in the surface temperature graphs (Figure 12), all four wall orientations maintained readings between 16.3 °C and 21.1 °C over the entire monitoring period. Even during peak daytime exterior heating, interior wall temperatures varied by less than 2 °C. The west-facing wall displayed the widest range (from 19.8 °C to 16.3 °C), while north- and south-facing interiors remained close to 17.5 °C–18.5 °C. This indicates that the core insulation layer effectively dampens temperature fluctuations, buffering the occupied space from external thermal dynamics. However, thermal imaging revealed local anomalies at floor junctions and fenestration edges, indicating potential thermal bridging (Figure 13). These bridges were spatially limited and did not significantly alter the overall interior temperature stability, but they highlight localized areas where detailing improvements could further enhance envelope performance.

Overall, this section reveals that the insulated rammed earth envelope functions as a dynamic thermal buffer. Exterior surfaces exposed to solar gain, especially those oriented south and east, exhibited strong absorptive and emissive behavior. Interior surfaces remained decoupled from these variations, offering stable indoor

FIGURE 7
UbiBot device mounted on a tripod at the center of the Main room for temperature and RH monitoring.

FIGURE 8
Observed snow coverage in front of the house from March 15 to 20, illustrating progressive snowmelt during the monitoring period.

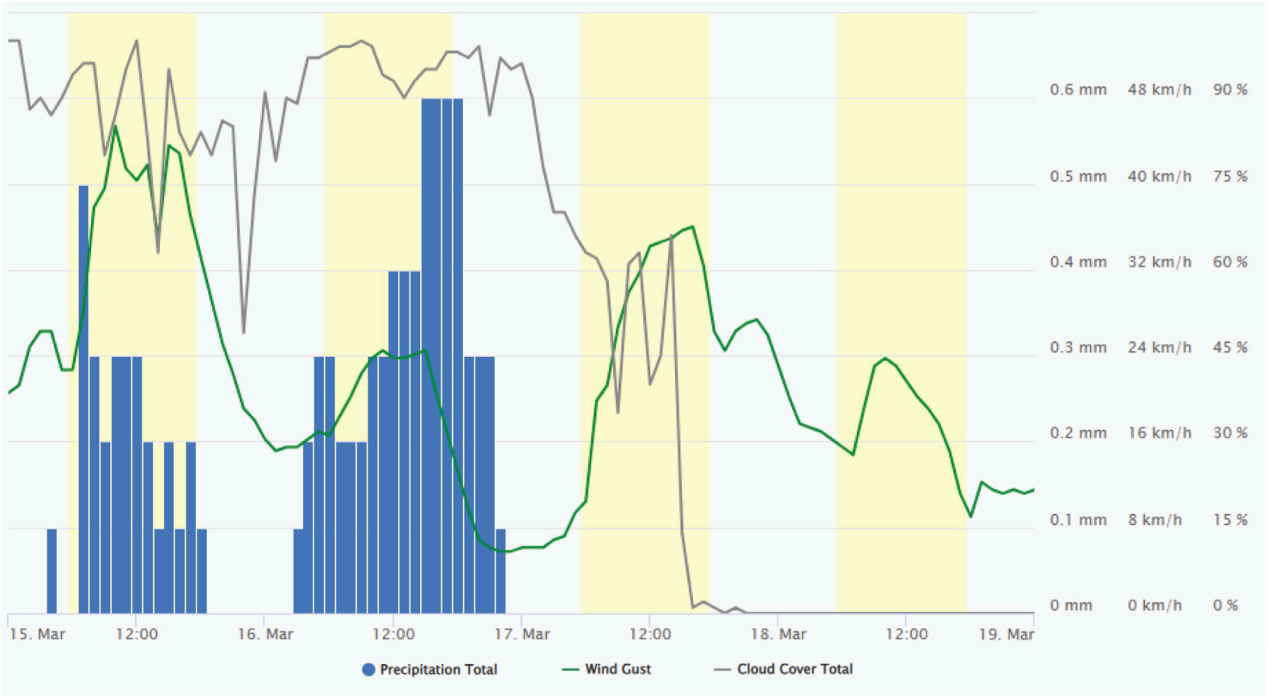

FIGURE 9
Climatic conditions recorded at hourly intervals from March 15 to March 19, showing wind speed, precipitation, and cloud cover based on data from Point Petre (AUT) ONT weather station (43.8395°N, 77.1515°W, 78.6°m; WIGOS ID 0-20000-0-71430).

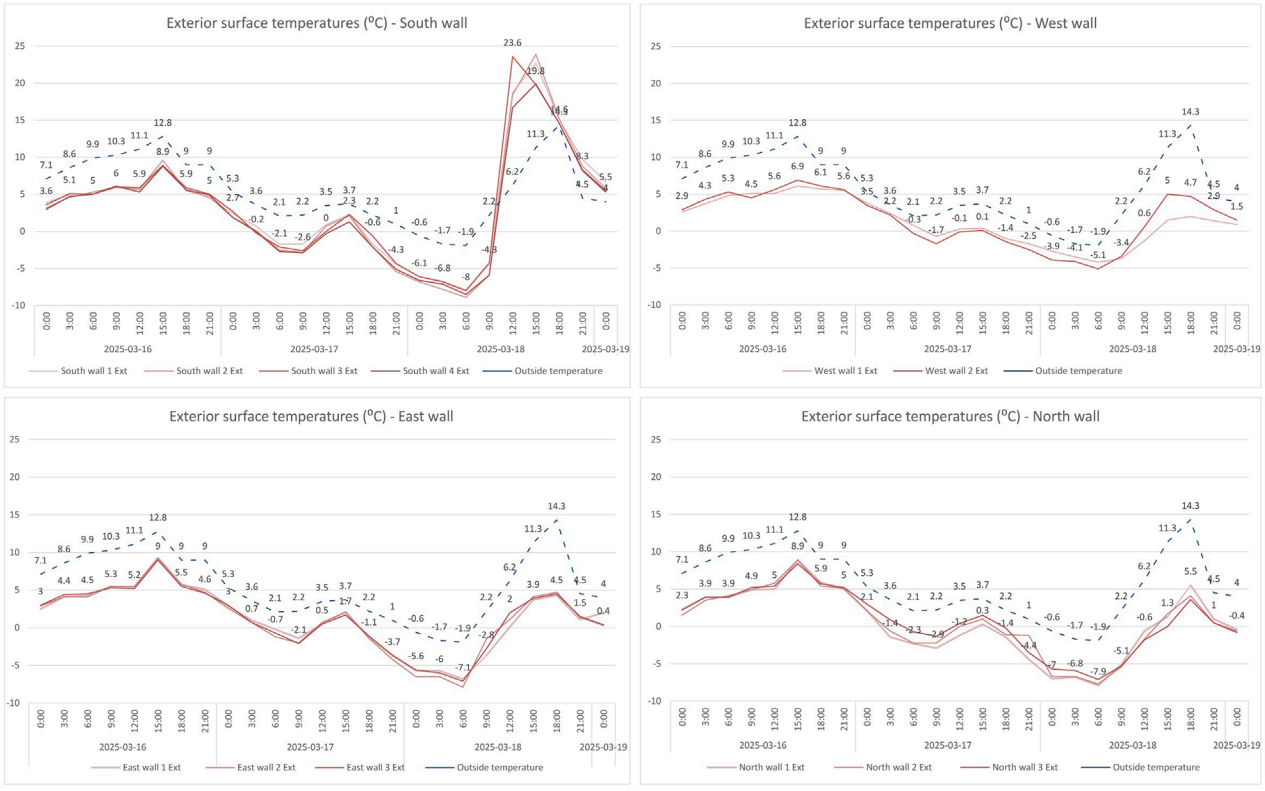

FIGURE 10
Exterior surface temperature trends for all four wall orientations compared to outdoor air temperature over the three-day monitoring period (March 16–18, 2025). Each graph shows temperature readings from multiple measurement points per façade.

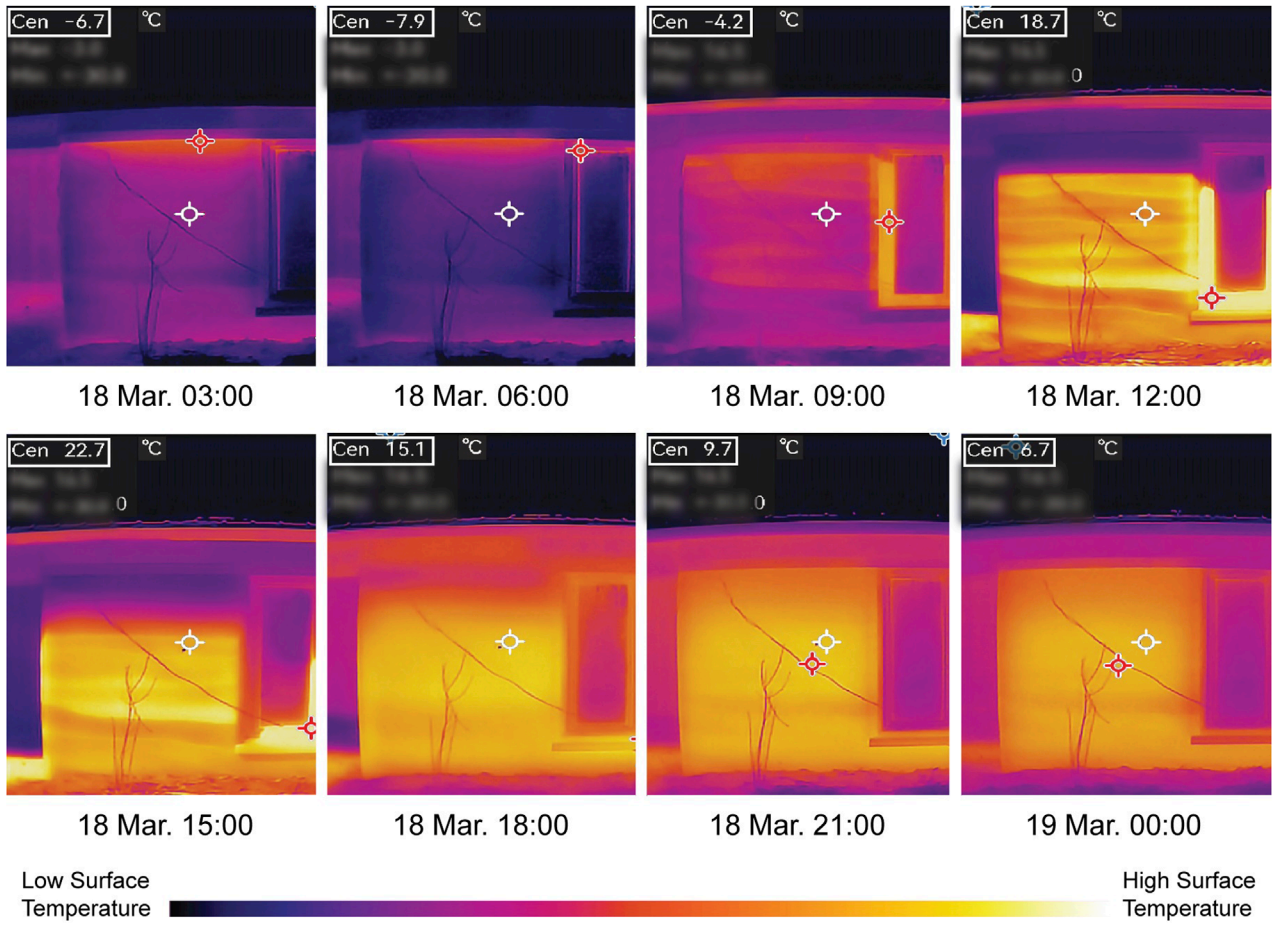

FIGURE 11
Sequence of IRT images captured on March 18 at 8 key intervals illustrating diurnal thermal behavior of the South wall 1 segment under passive conditions.

conditions and demonstrating the value of core insulation paired with exposed thermal mass.

3.2 Heat flux distribution and directional behavior

Heat flux measurements recorded on both the exterior and interior surfaces of the rammed earth walls provide insight into the directional energy exchanges occurring across all wall orientations during the unheated monitoring period. Values were logged at 3-h intervals between March 16 and 18, capturing variations driven by solar radiation, ambient temperature, and wall mass response.

On the exterior surfaces, surface temperatures measured via contact thermocouples embedded in the heat flux sensor plates remained above ambient air temperature for most of the monitoring period (Figure 14), leading to consistently negative heat flux values (Figure 15). These values indicate a net outward flow of heat from the warmer wall surface toward the colder external environment. Heat flux patterns exhibited strong diurnal and directional variation, particularly on March 16 and 17, when nighttime losses ranged from −5.2 to −8.4 W/m^2. The largest heat loss occurred on the north-facing wall, which remained shaded and cold throughout the period, acting as a continuous emitter in the absence of solar gain.

On March 18, the sunniest day, ambient air temperatures briefly exceeded wall surface temperatures on the east-, west-, and north-facing walls during early afternoon hours, resulting in short-lived positive heat flux peaks. These indicate a temporary inward flow of thermal energy from the warmer outdoor air to the slightly cooler wall surfaces. Maximum gains reached +3.84 W/m^2 on the north wall and +2.70 W/m^2 on the west wall. The south wall, in contrast, exhibited no positive heat flux values during this period. Its surface temperature peaked at 23.5 °C, approximately 9 °C above ambient, maintaining a consistent outward flux due to high solar absorption and delayed thermal re-emission.

Interior wall heat flux measurements remained low and stable across all orientations (Figure 15), ranging between −0.3 and +0.7 W/m^2 throughout the three-day period. These small magnitudes confirm the attenuating effect of the wall's core insulation layer and its thermal mass. Slight increases in interior heat flux were detected on March 18 in the afternoon, peaking at +0.7 W/m^2, particularly on south- and west-facing walls. These

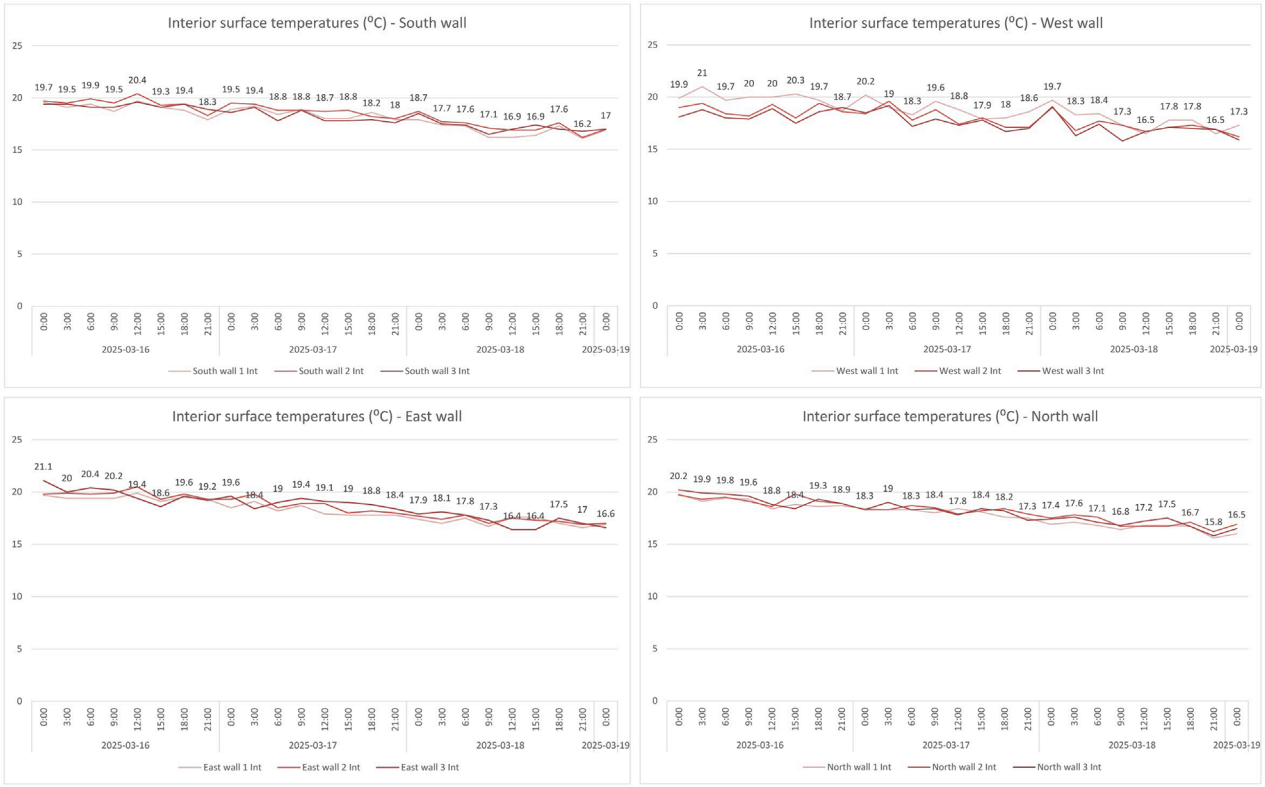

FIGURE 12
Interior surface temperatures (March 16–18, 2025) from three measurement points per wall, showing minimal diurnal fluctuation.

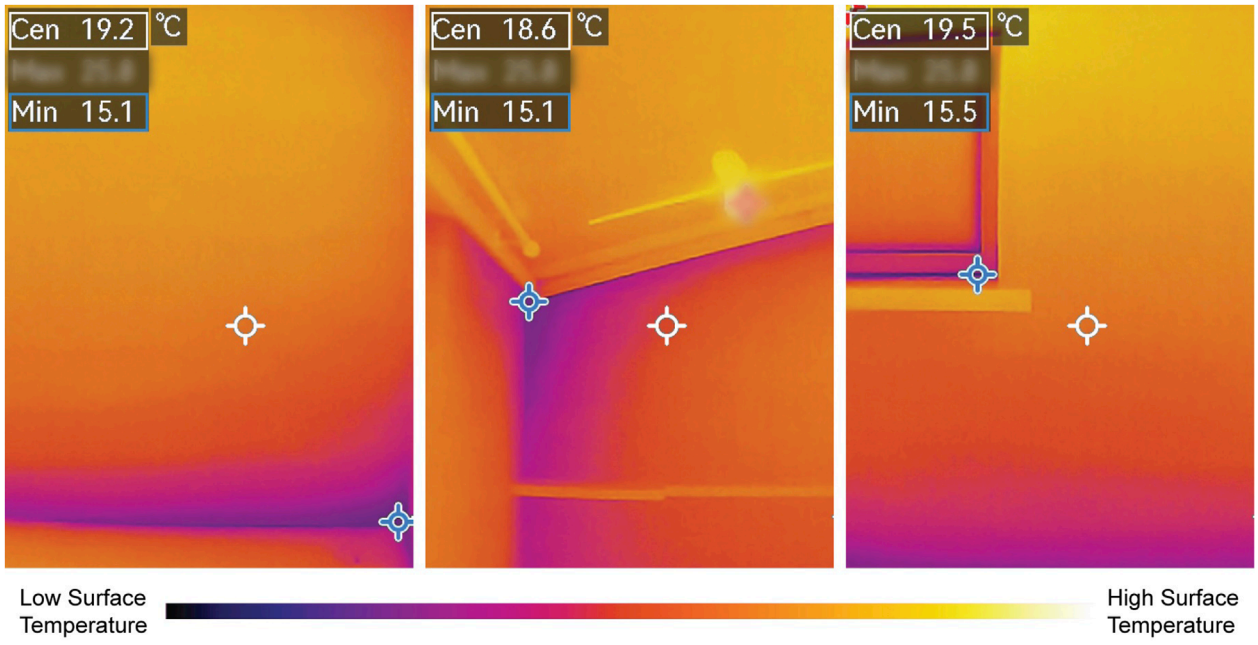

FIGURE 13
Thermal bridges observed during IRT monitoring detected at floor-to-wall junctions and around fenestration edges.

FIGURE 14
Exterior wall surface temperatures recorded via contact thermocouples embedded in heat flux sensors compared with ambient outdoor air temperature.

correspond to delayed transmission of stored solar heat from the wall core toward the interior space. However, the amplitude of these interior values remained more than an order of magnitude lower than those recorded externally, indicating effective buffering of internal conditions.

Together, these observations illustrate the composite wall system's ability to moderate directional energy flows. The exposed exterior surfaces interact dynamically with the environment, absorbing and releasing solar heat, while the insulated interior surfaces reduce the impact of short-term fluctuations. This dual behavior supports the passive design objective of achieving thermal stability through decoupled and time-shifted energy transmission.

3.3 Indoor temperature and humidity trends

Indoor environmental monitoring during the three-day unheated monitoring phase (March 16–18) demonstrated the stabilizing effect of the rammed earth envelope on interior thermal and moisture conditions. While exterior temperature dropped as low as −2.8 °C on the morning of March 17 and reached a daytime peak of 14.1 °C on March 18, indoor air temperatures remained within a narrow band of 19.0 °C–22.8 °C across all spaces, illustrating the envelope's buffering performance under passive operation (Figure 16).

The main room, located at the center of the house and adjacent to several wall orientations, showed the highest average temperature stability, ranging from 21.8 °C to 22.6 °C. The bathroom displayed slightly lower values, between 19.0 °C and 20.5 °C, likely due to reduced volume and limited solar exposure. Notably, the south room exhibited a brief peak near 22.8 °C in the afternoon of March 18, correlating with increased solar radiation following snowmelt (as shown in Figure 8), before gradually returning to baseline values by nightfall.

RH remained consistently stable indoors, fluctuating within a narrow range of 44%–52% (Figure 16). In contrast, exterior RH exhibited wide variation (from 65% to nearly 100%), particularly during snowmelt and clear sky conditions. The bathroom and north room recorded the highest indoor RH, around 50% on average, due to reduced solar exposure and lower air turnover. This consistent indoor RH, without mechanical ventilation or dehumidification, reflects the hygrothermal inertia of rammed earth, which likely contributed to moisture regulation through vapor buffering at the wall-air interface.

The observed trends support the hypothesis that the wall system contributes to interior thermal and moisture regulation during cold weather in the absence of active systems. The observed lag and attenuation between exterior and interior fluctuations underscore

FIGURE 15
Heat flux (W/m^2) measured on exterior and interior wall surfaces for all four orientations (March 16–18, 2025). Negative values represent outward heat flow from the wall to the environment, while positive values indicate inward flow from the ambient environment to the wall.

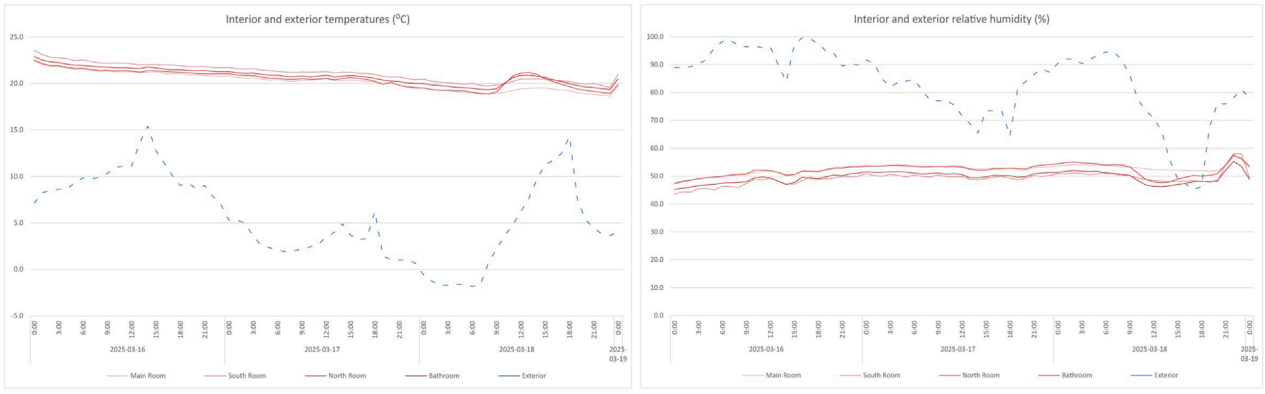

FIGURE 16
Indoor temperature and humidity during unheated period in four monitored rooms compared to exterior temperature (°C) and RH (%).

the role of material thermal mass in moderating internal comfort parameters in low energy buildings.

4 Discussion

This section interprets the experimental findings of the passive monitoring campaign in relation to existing literature on rammed earth construction, thermal inertia, and energy-efficient design in cold climates. The discussion focuses on five key aspects: thermal lag and time-shifted flux behavior, cold-climate thermal performance of stabilized rammed earth, measurement discrepancies between infrared thermography and embedded sensors, orientation-dependent envelope response and bioclimatic optimization, and thermal and hygrothermal buffering and comfort stability.

4.1 Thermal lag and time-shifted flux behavior

One of the most significant findings is the presence of a measurable thermal lag between exterior thermal excitation and interior response, particularly evident on the south wall. While exterior surface temperatures and heat fluxes peaked in the early afternoon, interior flux values rose with a delay of 2–3 h, and with significantly lower amplitude. This time shift reflects the envelope's capacity to absorb solar energy, store it within its thermal mass, and gradually re-emit it toward the interior. This behavior aligns with theoretical and empirical studies on phase shift and decrement delay in high-mass wall systems (Soudani et al., 2017; Taylor et al., 2008), and demonstrates its passive regulation value under winter conditions. In climates with pronounced diurnal variations, such time-lagged heat release aligns well with evening thermal demand patterns, reducing reliance on active heating systems (Givoni, 1994; Mazria, 1979).

4.2 Cold-climate performance and insulation strategy

Despite exterior temperatures dropping below −3 °C and solar availability varying across days, the interior surfaces and indoor air remained thermally stable (19.0 °C–22.8 °C), with minimal humidity fluctuation. This underscores the suitability of core-insulated, cement-stabilized rammed earth walls for cold-climate applications, confirming prior simulation-based predictions (Fix and Richman, 2009; Yu et al., 2022). The use of a core insulation layer not only preserves the thermal mass effect on the exterior face, allowing solar energy storage, but also decouples the interior surface from abrupt environmental changes, an approach shown to be more effective than external insulation in passive earth-based systems (Tinsley et al., 2019).

4.3 Sensor methods and measurement discrepancies

A notable divergence was observed between wall surface temperatures measured via IRT and those recorded by embedded heat flux sensors. IRT data often indicated lower-than-ambient nighttime values, especially under clear skies, while contact sensors recorded consistently higher temperatures. This is consistent with literature on IRT limitations: radiative surface temperature is affected by emissivity, cloud cover, and longwave sky radiation, often leading to underestimation during night hours (Kylili et al., 2014; Lucchi, 2018). In contrast, heat flux sensors embedded in contact plates capture conductive heat exchange at the material interface, providing a better estimate of thermal inertia. The dual instrumentation approach thus offers a fuller picture of surface and sub-surface dynamics, supporting best practices in hygrothermal envelope analysis (ISO 9869-1, 2014).

4.4 Orientation-dependent response and bioclimatic optimization

Clear asymmetries were observed between wall orientations, with south- and east-facing walls exhibiting stronger diurnal gains and thermal emission patterns than north-facing or shaded surfaces like the west-facing wall. The south wall reached surface peaks above 23 °C on March 18, 8 °C–10 °C above ambient, while the north wall remained under 7 °C. The west wall, partially shaded by an extensive roof overhang, displayed more moderate behavior: the solar-exposed segment showed patterns similar to the east wall and reached higher surface temperatures, whereas the shaded segment remained considerably cooler. This suggests that diurnal gains may still occur under limited solar exposure, with measurable temperature variations between different points along the same wall. These results are consistent with solar geometry and previous findings that emphasize orientation-specific design in passive strategies (Hasan and Dutta, 2015; Giuffrida et al., 2021; Dong et al., 2015). The absence of positive heat flux values on the south wall despite high surface temperatures indicates active solar gain and storage without risk of overheating the interior, due to the insulated core. These findings suggest that hybrid wall systems can be fine-tuned to harness solar radiation where available while minimizing losses in shaded zones, reinforcing orientation-aware design in massive envelopes.

4.5 Hygrothermal buffering and comfort stability

The observed indoor RH remained within a tight range (44%–52%) without active ventilation or dehumidification, even during snowmelt and exterior RH peaks nearing 100%. While cement stabilization may reduce wall permeability (Arrigoni et al., 2017), the envelope still demonstrated effective moisture buffering, likely due to porosity retained in the core and interior finishes. These results support earlier research (Hall and Allinson, 2012) which showed that massive, porous materials, even when stabilized, can moderate indoor humidity levels through passive vapor exchange, contributing to thermal comfort, improving indoor air quality and reducing reliance on the mechanical systems.

4.6 Conclusion

This exploratory case study examined the short-term thermal and hygrothermal behavior of a cement-stabilized, core-insulated rammed earth residence operating under free-running winter conditions in a cold climate. A multi-method field approach combining infrared thermography, surface heat-flux sensing, and *in-situ* environmental monitoring captured the dynamic response of a massive hybrid wall system under real climatic conditions. The results showed measurable thermal lag, reduced diurnal temperature swings, and delayed heat dissipation, confirming the envelope's ability to buffer interior conditions from outdoor variability.

Orientation proved critical: south- and east-facing façades exhibited strong solar responsiveness, while the shaded west and north façades remained comparatively inert. The integration of core insulation effectively decoupled indoor spaces from external fluctuations while maintaining the benefits of thermal mass. Differences between infrared thermography and heat-flux sensor data highlighted the complementary roles of radiative and conductive measurements in characterizing envelope behavior. Although localized thermal bridges were observed at floor-to-wall and wall-to-roof junctions and around window frames, their influence was limited to small surface areas and did not measurably affect the overall indoor temperature stability observed during the monitoring period. The core finding of this study, that the insulated rammed-earth wall system functions as an effective thermal and hygrothermal buffer, therefore, remains valid at the whole-building scale.

While the findings demonstrate the passive moderation potential of insulated rammed earth assemblies, the study's short duration and limited instrumentation restrict generalization beyond the monitored configuration. The work instead provides a rare, high-resolution dataset for validating future simulations and long-term monitoring of earthen envelopes in cold climates. Its main contribution lies in documenting real-world hygrothermal dynamics and establishing a methodological framework for reliable field-based characterization of low-carbon wall systems. Future research should extend monitoring to full seasonal cycles, include continuous energy-use tracking, and integrate calibrated simulations to explore variations in wall composition, insulation placement, and stabilization. Long-term studies on vapor diffusion, moisture buffering, and freeze–thaw resistance would further inform the design of durable, climate-responsive rammed earth buildings for cold regions.

Data availability statement

The datasets presented in this article are not readily available because they contain personal data. Requests to access the datasets should be directed to szende.szentesi-nejur@arc.ulaval.ca.

Author contributions

GH: Conceptualization, Data curation, Formal Analysis, Investigation, Methodology, Project administration, Resources, Visualization, Writing – original draft, Writing – review and editing. SS-N: Conceptualization, Data curation, Formal Analysis, Funding acquisition, Investigation, Methodology, Project administration, Resources, Software, Supervision, Validation, Visualization, Writing – original draft, Writing – review and editing.

Funding

The author(s) declare that no financial support was received for the research and/or publication of this article.

Acknowledgements

The authors gratefully acknowledge the Department of Mechanical Engineering at Université Laval for providing access to heat flux measurement equipment and for their technical support during the preparation phase of the monitoring campaign. Their guidance on the use of key instruments, including the thermal imaging camera and heat flux sensors, contributed significantly to the methodological rigor of this article. The authors also wish to express their appreciation to the School of Architecture at Université Laval for its support in facilitating this research, particularly through its academic infrastructure and commitment to advancing sustainable and experimental approaches to building envelope performance.

Conflict of interest

The authors declare that the research was conducted in the absence of any commercial or financial relationships that could be construed as a potential conflict of interest.

Generative AI statement

The author(s) declare that Generative AI was used in the creation of this manuscript. Minor language revisions were supported using ChatGPT (OpenAI) to improve clarity and consistency under full human oversight.

Any alternative text (alt text) provided alongside figures in this article has been generated by Frontiers with the support of artificial intelligence and reasonable efforts have been made to ensure accuracy, including review by the authors wherever possible. If you identify any issues, please contact us.

Publisher's note

References

Arrigoni, A., Grillet, A. C., Pelosato, R., Dotelli, G., Beckett, C. T. S., Woloszyn, M., et al. (2017). Reduction of rammed earth's hygroscopic performance under stabilisation: an experimental investigation. *Build. Environ.* 115, 358–367. doi:10.1016/j.buildenv.2017.01.034

Balaguer, L., Vegas López-Manzanares, F., Mileto, C., and García-Soriano, L. (2019). Assessment of the thermal behaviour of rammed Earth walls in the summer period. *Sustainability* 11 (7), 1924. doi:10.3390/su11071924

Beckett, C., and Ciancio, D. (2012). "A review of the contribution of thermal mass to thermal comfort in rammed Earth structures," in *ICSBE-2012: international conference on sustainable built environment*. Available online at: http://dl.lib.uom.lk/bitstream/handle/123/8924/SBE-12-48.pdf?sequence=1&isAllowed=y.

Beckett, C., Cardell-Oliver, R., Ciancio, D., and Huebner, C. (2017). Measured and simulated thermal behaviour in rammed Earth houses in a hot-arid climate. Part B comfort. *J. Build. Eng.* 13, 146–158. doi:10.1016/j.jobe.2017.07.013

Ciancio, D., and Beckett, C. (2015). "Thermal performance summary of four rammed earth walls in Canadian climates," *Rammed Earth construction* (The Netherlands: CRC Press/Balkema), 129–132. Available online at: https://www.taylorfrancis.com/books/9781315692944/chapters/10.1201/b18046-24.

Dong, X., Soebarto, V., and Griffith, M. (2014). Strategies for reducing heating and cooling loads of uninsulated rammed Earth Wall houses. *Energy Build.* 77, 323–331. doi:10.1016/j.enbuild.2014.03.031

Dong, X., Soebarto, V., and Griffith, M. (2015). Design optimization of insulated cavity rammed Earth walls for houses in Australia. *Energy Build.* 86, 852–863. doi:10.1016/j.enbuild.2014.11.014

Easton, D. (2007). "The rammed Earth house," in *White river junction*. 1st ed (Vermont: Chelsea Green Publishing Company), 407.

Fernandes, J., Mateus, R., Gervásio, H., Silva, S. M., and Bragança, L. (2019). Passive strategies used in southern Portugal vernacular rammed Earth buildings and their influence in thermal performance. *Renew. Energy* 142, 345–363. doi:10.1016/j.renene.2019.04.098

Fix, S., and Richman, R. (2009). *Viability of rammed Earth building construction in cold climates*, 18. Ontario, Canada: Toronto Metropolitan University. Available online at: https://chaenlnk.files.wordpress.com/2012/09/rammedearthforacoldclimate-stufix.pdf.

Giuffrida, G., Detommaso, M., Nocera, F., and Caponetto, R. (2021). Design optimisation strategies for solid rammed Earth walls in mediterranean climates. *Energies* 14 (2), 325. doi:10.3390/en14020325

Givoni, B. (1994). *Passive low energy cooling of buildings*. John Wiley and Sons.

Gupta, P., Cupkova, D., Ben-Alon, L., and Hameen, E. C. (2020). valuation of rammed Earth assemblies as thermal mass through whole-building simulation.

Hall, M., and Allinson, D. (2009). Assessing the effects of soil grading on the moisture content-dependent thermal conductivity of stabilised rammed Earth materials. *Appl. Therm. Eng.* 29 (4), 740–747. doi:10.1016/j.applthermaleng.2008.03.051

Hall, M., and Allinson, D. (2012). Humidity buffering using stabilised rammed Earth materials. *Proc. Institution Civ. Eng. - Constr. Mater.* 165 (6), 335–344. doi:10.1680/coma.11.00023

Hasan, M. M., and Dutta, K. (2015). "Investigation of energy performance of a rammed earth built commercial office building in three different climate zones of Australia," in *Rammed Earth construction: cutting-edge research on traditional and modern rammed Earth* (London, UK: Taylor and Francis Group).

Hutcheon, N. B., and Gop, H. (1995). *Building science for a cold climate*. 3rd ed. Canada: Institute for research in construction, 440.

ISO 6781-1 (2023). *Performance of buildings, detection of heat, air and moisture irregularities in buildings by infrared methods, part 3: equipment and image interpretation*. Geneva, Switzerland: International Organization for Standardization.

ISO 9869-1 (2014). *Thermal insulation, building elements, In-situ measurement of thermal resistance and thermal transmittance, part 1: heat flow meter method*. Geneva, Switzerland: International Organization for Standardization.

Jiang, B., Wu, T., Xia, W., and Liang, J. (2020). Hygrothermal performance of rammed Earth wall in Tibetan autonomous prefecture in Sichuan Province of China. *Build. Environ.* 181, 107128. doi:10.1016/j.buildenv.2020.107128

Kailey, A., and Rishi, G. (2015). Current state of modern rammed construction: a case study of first peoples house after seven years exposure. *KEM* 666, 63–76. doi:10.4028/www.scientific.net/kem.666.63

Krahn, T. (2019). *Essential rammed Earth construction*. 1st ed. Gabriola Island, British Columbia: New Society Publishers, 170.

Krayenhoff, M. (2012). "North American modern earth construction," in *Modern Earth buildings* (Vancouver, Canada: Woodhead Publishing), 561–608. Available online at: https://linkinghub.elsevier.com/retrieve/pii/B9780857090263500216.

Kylili, A., Fokaides, P. A., Christou, P., and Kalogirou, S. A. (2014). Infrared thermography (IRT) applications for building diagnostics: a review. *Appl. Energy* 134, 531–549. doi:10.1016/j.apenergy.2014.08.005

Lucchi, E. (2018). Applications of the infrared thermography in the energy audit of buildings: a review. *Renew. Sustain. Energy Rev.* 82, 3077–3090. doi:10.1016/j.rser.2017.10.031

Martin, M., Chong, A., Biljecki, F., and Miller, C. (2022). Infrared thermography in the built environment: a multi-scale review. *Renew. Sustain. Energy Rev.* 165, 112540. doi:10.1016/j.rser.2022.112540

Mazria, E. (1979). *The passive solar energy book: a complete guide to passive solar home, greenhouse, and building design. Emmaus, Pa*. NY, United States: Rodale Press.

Mellado, M. M. Á., Castilla Pascual, F. J., Pérez Andreu, V., and Gosalbo Guenot, G. A. (2021). Evaluation of the thermal comfort and energy demand in a building with rammed Earth walls in Spain: influence of the use of *in situ* measured thermal conductivity and estimated values. *Buildings* 11 (12), 635. doi:10.3390/buildings11120635

Narloch, P., Protchenko, K., and Cichocki, D. (2019). Hydro-thermal analysis of building envelope walls with cement-stabilized rammed Earth structural layer and different thermal insulators and their positioning in humid Continental climate. *IOP Conf. Ser. Mater Sci. Eng.* 661 (1), 012078. doi:10.1088/1757-899x/661/1/012078

Rempel, A. W., and Rempel, A. R. (2019). Frost resilience of stabilized Earth building materials. *Geosciences* 9 (8), 328. doi:10.3390/geosciences9080328

Samadianfard, S., and Toufigh, V. (2020). Energy use and thermal performance of rammed-earth materials. *J. Mater Civ. Eng.* 32 (10), 04020276. doi:10.1061/(asce)mt.1943-5533.0003364

Serrano, S., de Gracia, A., and Cabeza, L. F. (2016). Adaptation of rammed Earth to modern construction systems comparative study of thermal behavior under summer conditions. *Appl. Energy* 175, 180–188. doi:10.1016/j.apenergy.2016.05.010

Soudani, L., Woloszyn, M., Fabbri, A., Morel, J. C., and Grillet, A. C. (2017). Energy evaluation of rammed Earth walls using long term *in-situ* measurements. *Sol. Energy* 141, 70–80. doi:10.1016/j.solener.2016.11.002

Taylor, P., and Luther, M. B. (2004). Evaluating rammed Earth walls: a case study. *Sol. Energy* 76 (1–3), 79–84. doi:10.1016/j.solener.2003.08.026

Taylor, P., Fuller, R. J., and Luther, M. B. (2008). Energy use and thermal comfort in a rammed Earth office building. *Energy Build.* 40 (5), 793–800. doi:10.1016/j.enbuild.2007.05.013

Tinsley, J., and Pavía, S. (2019). Thermal performance and fitness of glacial till for rammed Earth construction. *J. Build. Eng.* 24, 100727. doi:10.1016/j.jobe.2019.02.019

Uprety, P., Shrestha, B., and Uprety, S. (2024). Energy performance of rammed earth building: a kathmandu valley case study. *J. Eng. Iss Solut.* 3 (1), 10–21. doi:10.3126/joeis.v3i1.64683

Verbeke, S., and Audenaert, A. (2018). Thermal inertia in buildings: a review of impacts across climate and building use. *Renew. Sustain. Energy Rev.* 82, 2300–2318. doi:10.1016/j.rser.2017.08.083

Wong, T., and Cook, S. (2014). "Insulated rammed Earth for a cold climate," in *Buildings for tomorrow* (Toronto). Available online at: https://obec.on.ca/CCBST2014/NEWS/index.php.

Yu, S., Hao, S., Mu, J., Tian, D., and Zhao, M. (2022). Research on optimization of the thermal performance of composite rammed Earth construction. *Energies* 15 (4), 1519. doi:10.3390/en15041519